Fluid dynamical simulations of coronavirus-laden respiratory droplets: Mind the wind and ambient air flows!

Simon Mendez, Alexandre Nicolas

Fluid dynamical simulations of coronavirus-laden respiratory droplets: Mind the wind and ambient air flows!

Simon MENDEZ*[1] and Alexandre NICOLAS†[2]

[1]IMAG, Univ. Montpellier, CNRS, Montpellier, F-34095, France
[2]Institut Lumière Matière, CNRS, Univ. Claude Bernard Lyon 1, Villeurbanne, F-69622, France

December 14, 2021

Abstract

The COVID-19 pandemic has prompted numerous fluid dynamical simulations of the propagation of potentially virus-laden respiratory droplets. While these studies have highlighted the apparent sensitivity of the numerical results to the sizes of the emitted droplet and the local humidity, many of them are still performed in stagnant air, i.e., without any external air flow. This very short note demonstrates, on the basis of coarse-grained fluid dynamical simulations in a simple generic setting, that even modest winds or air draughts strongly impact the risks of short-ranged transmission via droplets. The induced dispersion of droplets may contribute to explaining the lower risks of viral transmission experienced outdoors, even at short range.

1 Context

The current COVID-19 pandemic has prompted computational fluid dynamical (CFD) studies galore to better understand the propagation of potentially virus-laden respiratory droplets and/or examine the scientific basis of social distancing guidelines [1, 2, 3, 4, 5]. The sensitivity of this propagation to several environmental factors, including temperature, humidity and wind [2, 6], as well as to the actual sizes of emitted droplets [7], has been underscored in recent publications. In this brief note, we emphasise the paramount effect of air flows, even at very moderate speeds, on the dispersion of respiratory droplets. This raises the question of the use of stagnant air conditions to simulate short-range viral transmissions in outdoor settings or even in well ventilated indoor settings. It may also rationalise the lower risks of viral transmission supposedly associated with outdoor settings.

A longer and more detailed report of these results will follow, notably detailing the effect of walking and applying the methods to larger-scale risk assessment.

2 Methods

We conducted a series of CFD simulations following the method described in Appendix A. In short, a still-standing manikin mimics a human being who is breathing through the mouth, at a rate of 20 breaths of 1 L of volume per minute, i.e., one breath every 3 seconds, with an equal time for exhalation and inhalation. This signal was originally designed to replicate the breathing flow rate of a walking person. Large-eddy simulations are performed as already reported in [8, 9] and detailed in the appendix, using the incompressible version of the Navier-Stokes equations. Droplets of diameters uniformly distributed in $d \in [0.1\,\mu\text{m}, 5\,\mu\text{m}]$ are injected into the airflow exhaled by the emitter. Note that the number of injected droplets (about 6,000 per breath) is not intended to be consistent with the actual number of particles emitted while breathing [10, 11], but

*Email: simon.mendez@umontpellier.fr
†Email: alexandre.nicolas@polytechnique.edu

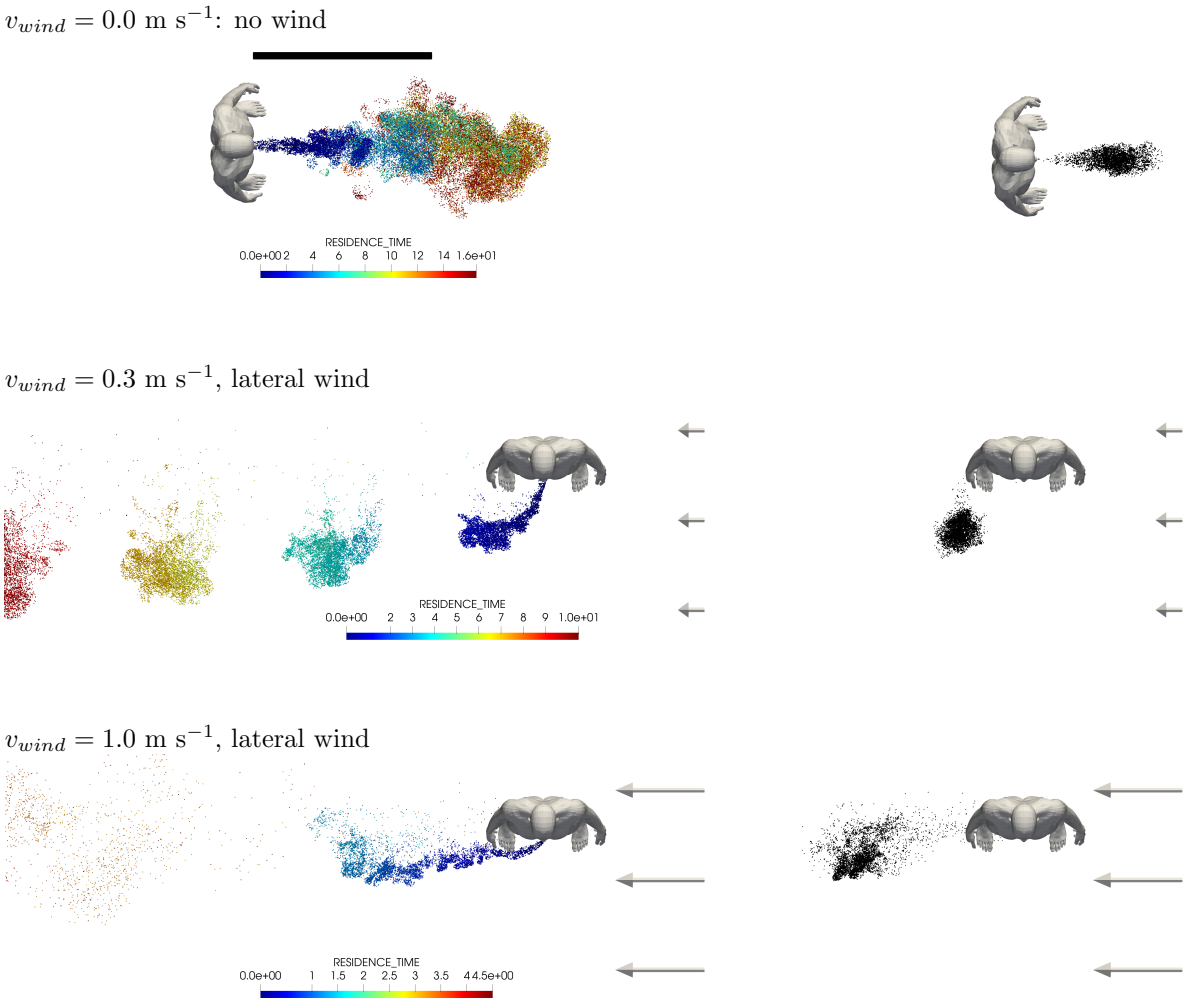

Figure 1: Clouds of particles mimicking the aerosols exhaled by the emitter, simulated with CFD for different wind speeds and widn directions. Each row corresponds to a different condition. *Images on the left*: cloud of particles at t=16.5 s after the beginning of the simulation (at the end of the exhalation of the 6$^{\text{th}}$ cycle), coloured by their residence time (note the different colour scales for each condition). *Images on the right*: Cumulated cloud of particles emitted 1.0 s$\pm$0.1 s before the observation time, corresponding to a delay $\tau = 1.0$ s in Fig. 2. The scale is the same for all images, with the black bar in the top left corner representing 1 m. Arrows represent the incident wind flow.

merely to collect sufficient statistics in terms of particles behaviour over a few cycles. Any actual distribution of emitted droplet sizes can then be obtained by simple rescaling; our results will be illustrated using the empirical distribution associated with the breathing mode measured by [12], which is sharply peaked around 0.8 μm.

In our reference settings, thermal effects and evaporation are discarded. In this note, the wind is assumed to blow in the direction perpendicular to the head orientation of the emitter, even though we have explored a much broader range of situations. Wind is modelled as a perfectly uniform flow. This means that velocity gradients in the height direction are neglected, considering that the wind speed which matters is that at the height of the head of the emitter. In addition, no exogenous turbulence is added to the incident wind flow to simplify the analysis.

Figure 1 shows the clouds of particles emitted after the exhalation of the 6$^{\text{th}}$ cycle (left images), or at a given time delay after their emission (right panels), for different wind speeds ranging from 0.0 to 1.0 m $\cdot$ s^{-1}.

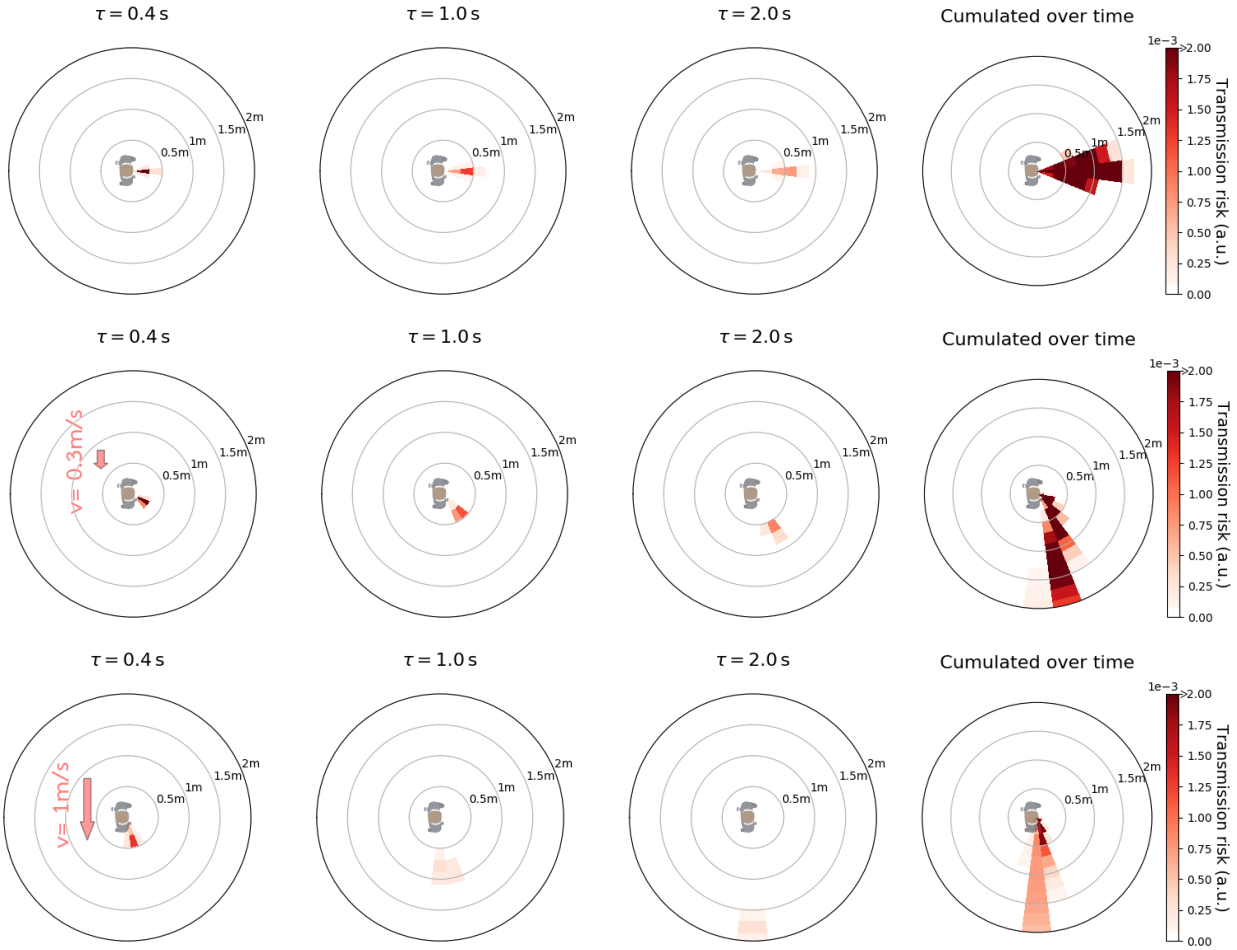

Figure 2: Spatio-temporal diagram of risks for different wind speeds, for a wind direction perpendicular to the head orientation.

Note that all speeds are very low and would not even qualify for a description as 'light breeze'. A wind of $1.0\,\mathrm{m}\cdot\mathrm{s}^{-1}$ corresponds to the air flow felt when walking in a still environment. For the cases with wind, particles are substantially deviated from the direction in which they were emitted, even only 1.0 s after their emission.

To facilitate the interpretation of the simulation output, we coarse-grain the results by calculating the total volume of respiratory fluid in polar grid cells centred around the emitter's head, only keeping the droplets that are within $\pm 20\,\mathrm{cm}$ of the altitude of the emitter's mouth. Furthermore, the droplets are binned into time intervals representing the delay after their emission. The method is described in Appendix D of [9]; it relies on the assumption that viral copies are homogeneously distributed in respiratory fluids and each raises the same risk of infection (regardless of the droplet size). The ensuing spatio-temporal diagrams of risks are presented in Fig. 2. The effect of ambient air flows is particularly visible in its influence on the direction of the exhaled jet.

While it might be important to improve our knowledge of the distribution of emitted droplet sizes and better describe the effect of temperature and humidity, auxiliary tests have yielded that the exact droplet size (below $20\,\mu\mathrm{m}$) and evaporation affect the transport of droplets far less than air flows. The latter even seem to prevail over thermal effects. Note however that our conclusions do not apply for larger inertial particles, whose dynamics are dominated by their initial momentum and gravity.

As stated early in 2020 [6], it might be that wind and air flows convey droplets farther over short periods of time, but their primary effect, even at barely detectable speeds, is to disperse these droplets. This is

demonstrated in Fig. 3, where we plot the decay of the time-cumulated viral concentration (in arbitrary units) with distance for different wind speeds, at the azimuthal angle where this concentration is found maximal. A wind speed as low as 0.3 m/s reduces the peak value at 50-cm distance by a factor of ∼3.

3 Conclusions

All these results point to the paramount importance of air flows for the propagation of respiratory droplets and warn against the incautious use of stagnant-air conditions if quantitative results are sought. This effect of air flows has been reported previously in case studies of specific (mostly indoor) settings [13, 14, 15, 16, 17, 18]; its generality is highlighted here.

These findings may contribute to explaining why overall outdoor settings appear to raise substantially fewer risks of viral transmission than enclosed spaces, in addition to the negligible risk of long-range air-borne transmission in non-confined settings.

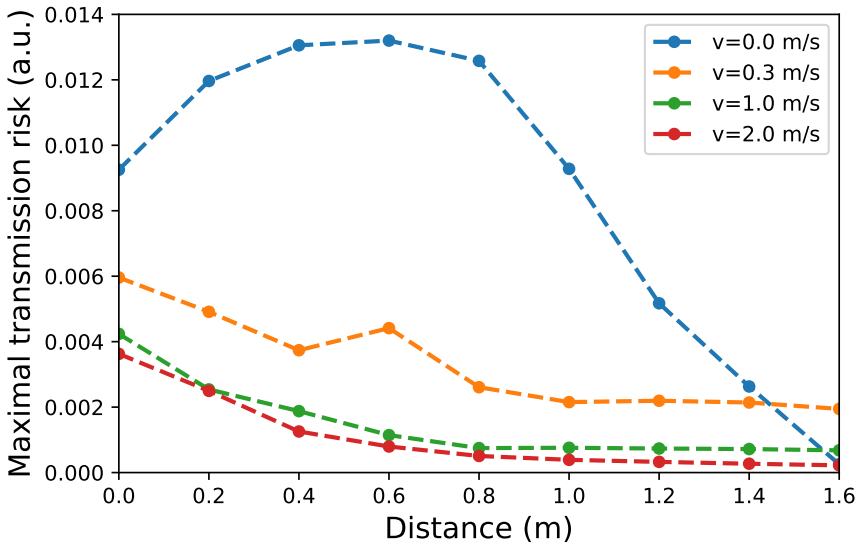

Figure 3: Radial decay of the maximum concentration of viral particles over all azimuthal directions, for winds blowing perpendicularly to the head orientation, at different speeds. The risk of transmission is assumed to be proportional the the local concentration of virus-laden droplet fluid found at the typical height of an adult.

Acknowledgments

The setup of the CFD simulations was designed collectively, with P. Bénard, G. Lartigue, V. Moureau (CORIA Rouen, France), G. Balarac, P. Bégou (LEGI Grenoble, France), Y. Dubief (Univ. Vermont, USA) and R. Mercier (Safran Tech, France). CFD simulations were performed using HPC resources from TGCC-IRENE (Grants No. AP010312425 and A0100312498).

References

[1] F. Yang, A. A. Pahlavan, S. Mendez, M. Abkarian, and H. A. Stone, "Towards improved social distancing guidelines: Space and time dependence of virus transmission from speech-driven aerosol transport between two individuals," *Physical Review Fluids*, vol. 5, no. 12, p. 122501, 2020.

[2] K. L. Chong, C. S. Ng, N. Hori, R. Yang, R. Verzicco, and D. Lohse, "Extended Lifetime of Respiratory Droplets in a Turbulent Vapor Puff and Its Implications on Airborne Disease Transmission," *Physical Review Letters*, vol. 126, jan 2021.

[3] G. Cortellessa, L. Stabile, F. Arpino, D. E. Faleiros, W. van den Bos, L. Morawska, and G. Buonanno, "Close proximity risk assessment for SARS-CoV-2 infection," *Science of The Total Environment*, vol. 794, p. 148749, 11 2021.

[4] A. Giri, N. Biswas, D. L. Chase, N. Xue, M. Abkarian, S. Mendez, S. Saha, and H. A. Stone, "Colliding respiratory jets as a mechanism of air exchange and pathogen transport during conversations," *Journal of Fluid Mechanics*, vol. 930, p. R1, 2022.

[5] A. Fabregat, F. Gisbert, A. Vernet, S. Dutta, K. Mittal, and J. Pallarès, "Direct numerical simulation of the turbulent flow generated during a violent expiratory event," *Physics of Fluids*, vol. 33, no. 3, p. 035122, 2021.

[6] Y. Feng, T. Marchal, T. Sperry, and H. Yi, "Influence of wind and relative humidity on the social distancing effectiveness to prevent COVID-19 airborne transmission: A numerical study," *Journal of Aerosol Science*, p. 105585, 2020.

[7] M. Rosti, S. Olivieri, M. Cavaiola, A. Seminara, and A. Mazzino, "Fluid dynamics of COVID-19 airborne infection suggests urgent data for a scientific design of social distancing," *Scientific reports*, vol. 10, no. 1, pp. 1–9, 2020.

[8] M. Abkarian, S. Mendez, N. Xue, F. Yang, and H. A. Stone, "Speech can produce jet-like transport relevant to asymptomatic spreading of virus," *Proceedings of the National Academy of Sciences*, vol. 117, no. 41, pp. 25237–25245, 2020.

[9] W. Garcia, S. Mendez, B. Fray, and A. Nicolas, "Model-based assessment of the risks of viral transmission in non-confined crowds," *Safety Science*, vol. 144, p. 105453, 2021.

[10] S. Asadi, C. D. Cappa, S. Barreda, A. S. Wexler, N. M. Bouvier, and W. D. Ristenpart, "Efficacy of masks and face coverings in controlling outward aerosol particle emission from expiratory activities," *Scientific reports*, vol. 10, no. 1, pp. 1–13, 2020.

[11] M. Alsved, A. Matamis, R. Bohlin, M. Richter, P. Bengtsson, and C. Fraenkel, "Exhaled respiratory particles during singing and talking," *Aerosol Science and Technology*, 2020.

[12] G. Johnson, L. Morawska, Z. Ristovski, M. Hargreaves, K. Mengersen, C. Y. H. Chao, M. Wan, Y. Li, X. Xie, D. Katoshevski, *et al.*, "Modality of human expired aerosol size distributions," *Journal of Aerosol Science*, vol. 42, no. 12, pp. 839–851, 2011.

[13] Y. Li, H. Qian, J. Hang, X. Chen, L. Hong, P. Liang, J. Li, S. Xiao, J. Wei, L. Liu, *et al.*, "Evidence for probable aerosol transmission of SARS-CoV-2 in a poorly ventilated restaurant," *medRxiv*, 2020.

[14] V. Vuorinen, M. Aarnio, M. Alava, V. Alopaeus, N. Atanasova, M. Auvinen, N. Balasubramanian, H. Bordbar, P. Erästö, R. Grande, *et al.*, "Modelling aerosol transport and virus exposure with numerical simulations in relation to SARS-CoV-2 transmission by inhalation indoors," *Safety Science*, vol. 130, p. 104866, 2020.

[15] F. Poydenot, I. Abdourahamane, E. Caplain, S. Der, J. Haiech, A. Jallon, I. Khoutami, A. Loucif, E. Marinov, and B. Andreotti, "Risk assessment for long and short range airborne transmission of sars-cov-2, indoors and outdoors, using carbon dioxide measurements," *arXiv preprint arXiv:2106.09489*, 2021.

[16] Mariam, A. Magar, M. Joshi, P. S. Rajagopal, A. Khan, M. M. Rao, and B. K. Sapra, "CFD simulation of the airborne transmission of COVID-19 vectors emitted during respiratory mechanisms: Revisiting the concept of safe distance," *ACS Omega*, 2021.

[17] I. Mills and F. Hamad, "A review and CFD case study: The effect of temperature, humidity, aerodynamics on corona virus transmission, mitigation in open and enclosed environments," *Biomedical Journal of Scientific & Technical Research (BJSTR)*, 2021.

[18] E. Rivas, J. L. Santiago, F. Martín, and A. Martilli, "Impact of natural ventilation on exposure to sars-cov 2 in indoor/semi-indoor terraces using co2 concentrations as a proxy," *Journal of Building Engineering*, vol. 46, p. 103725, 2022.

[19] V. Zmijanovic, S. Mendez, V. Moureau, and F. Nicoud, "About the numerical robustness of biomedical benchmark cases: Interlaboratory FDA's idealized medical device," *International journal for numerical methods in biomedical engineering*, vol. 33, no. 1, pp. e02789:1–17, 2017.

[20] V. Moureau, P. Domingo, and L. Vervisch, "Design of a massively parallel CFD code for complex geometries," *Comptes Rendus Mécanique*, vol. 339, no. 2-3, pp. 141–148, 2011.

[21] V. Moureau, P. Domingo, and L. Vervisch, "From large-eddy simulation to direct numerical simulation of a lean premixed swirl flame: Filtered laminar flame-PDF modelling," *Combustion and Flame*, vol. 158, pp. 1340–1357, 2011.

[22] J. K. Gupta, C.-H. Lin, and Q. Chen, "Characterizing exhaled airflow from breathing and talking," *Indoor air*, vol. 20, no. 1, pp. 31–39, 2010.

A Appendix: Numerical method and simulations details

Physical model and flow solver

Three-dimensional numerical simulations are performed in the idealised case of non-buoyant jets, neglecting temperature effects. To account for turbulence, we use Large Eddy Simulations (LES) as already reported and described in [8].

Particles are moved by integrating Newton's law, with external forces limited to gravity and to a simple model of drag that accounts for the difference in speed between the particle and the surrounding fluid. In practice, as particles smaller than 5 microns in diameter are considered, their trajectory is close to that of tracers.

The flow solver YALES2 [8, 19] was used in the present work (https://www.coria-cfd.fr/index.php/YALES2). The fluid equations are discretised using a fourth-order finite-volume scheme, adapted to unstructured grids [20, 21].

Computational domain and grid

The computational domain is a box of size $L_x = 4$ m, $L_y = 3$ m and $L_z = 6$ m, where y is the vertical direction (with gravity along $-y$) and (x,z) is the horizontal plane. The manikin's head is oriented in the $-x$ direction and the wind blows in the $-z$ direction.

The grid is initially refined around the head of the manikin with a spatial resolution of 1 mm and coarsened further. A dynamic mesh adaptation algorithm is used to refine the grid wherever needed. To do so, a passive scalar is injected at the mouth. Any location where the concentration of this passive scalar is non-zero is identified as a meaningful region and the grid is subsequently refined during the calculation, with a target grid size of 8 mm.

Boundary conditions

The in-flow boundary condition is located at the $+z$ end of the domain, where a uniform flow of $\vec{v} = (0, 0, -v_{wind})$ is assumed. Slipping wall boundary conditions are applied to the lateral boundaries, and the outflow boundary condition is applied at the $-z$ end of the domain.

The flow is injected at the manikin's mouth, which has been delimited by hand as the surface covered by the lips of the manikin, whose mouth is initially closed. This yields a non-planar surface of 4.7 cm^2 on which a uniform velocity is imposed, parallel to the ground and in front of the manikin.

The time signal is periodic, with a period of 3.0 s, and was designed to mimic a breathing signal [22] with a short period typical of the breathing pace while walking.

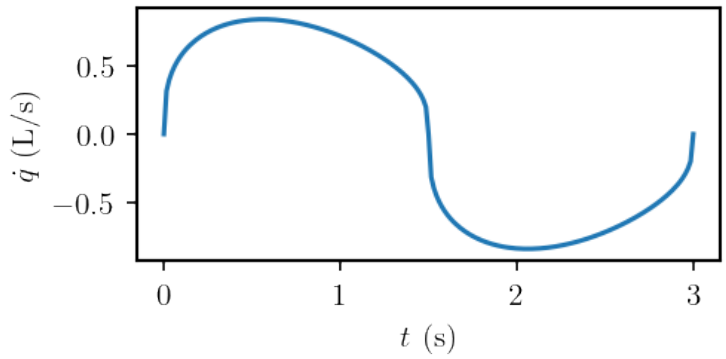

Figure S1: Flow rate imposed at the mouth of the manikin at each cycle of duration 3.0 s.

Simulations

Simulations are first performed over a small number of cycles to install the flow. The number of cycles differs depending on the wind velocity (from 2 for high-speed cases to 4 in the case without wind). Then, 4 cycles are computed to collect the statistics presented in Fig. 2 and Fig. 3. Solutions are stored every 0.25 s (12 par cycle) for statistical accumulation.